

# Cost of Energy Assessment Methodology for offshore AC and DC wind power plants

Dumitru-Mihai Valcan  
duval@vestas.com

Philip Carne Kjær  
pck@vestas.com

Lars Helle  
lah@vestas.com

Sridhar Sahukari  
srisa@vestas.com

Mohamed Haj-Maharsi  
mohma@vestas.com

Sunita Singh  
sumal@vestas.com

Vestas Wind Systems A/S

**Abstract**—In offshore wind power plants, the losses occurring in the path from the wind turbine to the point of common coupling contribute significantly to the cost of energy. Therefore, a reduction of the losses along this path represents a desirable way to drive down the energy cost. For state-of-the-art AC systems, simply increasing the voltage level in the collection grid has the potential of improving its efficiency. However, since large offshore wind power plants tend towards being connected to shore through HVDC transmission lines, one might extend the DC nature of the high voltage transmission to the collection grid in the attempt of reducing the losses. Nevertheless, both solutions may increase the cost of the system and therefore, their potential benefits must be quantified in the proper way and as accurate as possible. This paper presents a tool to assess the performance of different wind power plant configurations in order to suggest the most appropriate solutions for offshore applications. The advantages of this tool are expressed in terms of configurability, fast computation and increased automation level. The assessment presented in this paper is intended to highlight the potential benefits of adopting DC technologies for offshore wind power developments and the proposed methodology is exemplified by a study case where a standard AC configuration is compared with alternative DC solutions.

**Keywords:** DC collection grid, DC wind turbine, WPP efficiency assessment, HVDC grids, cost of energy, offshore super grid, Dual Active Bridge, Single Active Bridge.

## I. INTRODUCTION

Wind power generation capacity is continuously increasing, encouraged by the global trend to reduce the greenhouse gas emissions [1]-[3]. Currently, Europe is the world leader in offshore wind power with a total installed capacity of 4 GW. The UK only, provides the potential to deliver 47 GW of offshore wind power generation, with *Round 3* being the start of the biggest offshore wind power development program in the world.

According to [4] there are 25 GW of planned offshore wind power projects in UK by 2020. Since many of these projects are located at a considerably long distance from the shore, it is foreseen that HVDC transmission technology will be used for the connection to the main grid due to its advantages compared to conventional AC transmission [5]-[14].

The cost associated with development of these new projects is rather high due to (among other reasons) long distances to their location, increased water depths and demand for new

technological developments such as new wind turbines (WT) with increased capacity. The cost of development is strongly related to the so called Cost of Energy (CoE), which is probably the most important factor when assessing electric energy production systems. It is therefore imperative to find methods that will drive down the CoE in order to make wind power competitive with conventional power generation systems.

One possible approach in the attempt of reducing the CoE is to reduce the overall losses in the system. The first step towards loss reduction in offshore wind power plants (WPP) is to increase the AC voltage level in the collection grid. Presently, the AC voltage level adopted for the offshore WPP collection grids is typically 20 kV across Europe and 33 kV in the UK.

Another approach that was extensively investigated is to build a DC collection grid. Such a collection grid would operate at medium voltage (MV) and would have the main benefit of reducing the losses in the system, making the CoE reduction possible. A big advantage of adopting DC collection grids is that it allows for weight savings of the components used in the system.

Obviously, a DC collection grid would require modifications of the WTs in order to output DC power and will impose the use of an offshore substation that makes use of DC/DC converters. Several approaches can be used to build a WT with DC output [15]-[18]. Simply removing the grid side converter of a full-scale back-to-back converter [19] will allow the WT to provide DC output in a low voltage range (0.5kV – 1.5kV). However, this voltage level is most probably not high enough to assure a reduction of losses in the collection grid. Therefore, it has to be raised to a higher value (i.e. MV) using a DC/DC converter [20]-[26] or by connecting wind turbines in series until the transmission voltage level is reached [27]-[29].

Regardless the adopted approach (i.e. increasing the AC voltage level or switching to DC technology), the overall cost of the system might increase. Therefore, the benefits associated with certain technology options must be properly quantified and as accurate as possible. When evaluating different system configurations there are several important elements that must be considered for determining their overall

impact on the CoE. These elements are: initial capital cost (ICC), operations and maintenance cost (O&M), leveled replacement cost (LRC), and annual energy production (AEP). Consequently, there is a need for an evaluation methodology that takes into consideration all these factors.

Building on the tradition of previous research work in this area [30]-[35], this paper presents a new CoE evaluation tool for AC and DC offshore WPPs. The tool is intended to be helpful in assessing the benefits of adopting DC technologies compared to conventional AC solutions. The analysis performed by the CoE tool involves the combined effect of WT aspects, collection grid aspects and substation aspects. The only part of the transmission technology considered in this work is the offshore substation, which is prone to modifications when a DC collection grid is adopted (assuming an HVDC connection to the main grid).

In addition to previous related work, the CoE tool presented in this paper brings several advantages such as increased flexibility, configurability and automation level, but also faster computation. All these are very important when a large number of configurations need to be assessed. The above mentioned advantages come from the method used for calculating the parameters that form the CoE, especially the approach taken to calculate the losses in the power electronic conversion system of the WT and substation. This will be explained in the following sections.

The tool has been exemplified with a study case for an 800 MW offshore WPP consisting of 100 WTs rated 8 MW each, where a conventional base case AC WPP has been compared with several DC WPP configurations.

## II. BACKGROUND ON CoE CALCULATION

As it was previously explained, the CoE tool described in this paper presents several important advantages when it comes to evaluating a large number of system configurations.

The reason for that lies on the way the tool is built. In the following sections each component involved in the CoE calculation will be described.

The CoE is determined based on [34] as the aggregated cost of the WPP divided by the annual energy production of the WPP, and is expressed by the following equation.

$$CoE = \frac{AC_{WPP}}{AEP_{WPP}} \quad (1)$$

### A. Aggregated cost of the WPP

As seen in Fig. 1, the aggregated cost of the WPP mainly consists of fixed and variable components and is detailed below.

$$AC_{WPP} = (1 + FCR) \cdot ICC + LRC + O\&M \quad (2)$$

$$ICC = \frac{ICC_{WTs} + ICC_{CG} + ICC_{SS}}{LT_{WPP}} \quad (3)$$

In the above formulas, the following notations have been adopted:

- $AC_{WPP}$  is the aggregated cost of the WPP;
- $AEP_{WPP}$  is the WPP annual energy production;
- $LT_{WPP}$  is the WPP lifetime;
- $FCR$  (fixed charge rate), representing a percentage of the initial capital cost which includes construction financing, financing fees, return on debt and equity, depreciation, income tax, and property tax and insurance;
- $ICC$  (initial capital cost of the WPP per year), which considers the WTs cost, collection grid cost and substation cost as seen in the equation below;
- $LRC$  (leveled replacement cost per year) distributes the cost of major replacements over the life of the wind turbine and is expressed in \$/kW

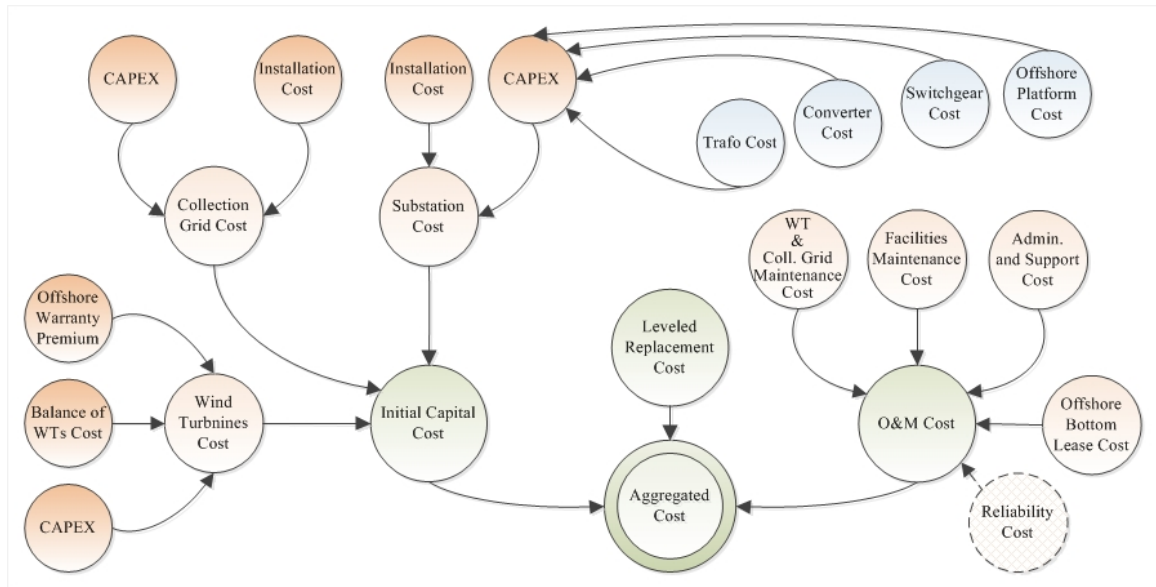


Fig. 1. Components forming the Aggregated cost.

machine rating;

- *O&M* (operation & maintenance cost per year) which includes costs related to scheduled and unscheduled turbine maintenance, facilities maintenance, administration and support. The cost associated with the offshore bottom lease was also included here.
- $ICC_{WTs}$  (initial capital cost of the WT) which contain the WT's CAPEX and the balance of WT cost. There is also an offshore warranty premium included in the initial capital cost of the WT's, which is a percentage of the WT's value. The balance of WT cost contains all the costs related to foundation, support structure, transportation, port and staging equipment, turbine installation permits, personnel access, scour protection and electrical interface connection;
- $ICC_{CG}$  (initial capital cost of the collection grid) which contains the collection grid CAPEX and installation cost;
- $ICC_{SS}$  (initial capital cost of the substation) which contains the substation CAPEX and installation cost. The substation CAPEX comprises the cost of the offshore platform, switchgear, and converter and transformer.

The numbers forming the aggregated cost can be obtained based on cost scaling curves for all the major components of the WPP, as described in [34]. This should be exercised for a base case scenario of given configuration rating, in which the cost for all the major components (e.g. WT, substation and collection grid) must be determined. The cost associated with all the other configurations that need to be assessed can be obtained using the following procedure.

Firstly, one must identify what changes the new system configuration will bring to the base case scenario, such as components/subsystems that will have different designs. Once the changes are identified, the bill of materials (BOM) cost of the component/subsystem causing the changes must be calculated. In the same time, the BOM cost of the new component/subsystem that will be used in the new configuration must be obtained. By interchanging the two component/subsystem BOM costs, one can obtain the aggregated cost for new system configurations.

The BOM cost for particular components of the system is determined based on detailed design work which allows the selection of components with appropriate ratings for predefined operating conditions. The following equation shows how the aggregated cost for new system configurations can be obtained.

$$\begin{aligned}
 & \text{Aggregated cost of the NEW SYSTEM} \\
 &= \text{Aggregated cost of the BASE CASE SYSTEM} \\
 &- \text{BOM of the component in the BASE CASE SYSTEM} \quad (4) \\
 &+ \text{BOM of the component used in the NEW SYSTEM}
 \end{aligned}$$

For correctly determining the aggregated cost of new system configurations, the BOM cost of the affected component must be accurately determined. This might be a source of error if accurate cost data is not available. The BOM cost of certain components or subsystems can be obtained from cost scaling models if more accurate sources are not available. However, in this paper most of the costs forming the BOM were obtained from vendor quotes. Where vendor quotes were not available, costs were derived and scaled from related areas.

### B. Annual Energy Production of the WPP

The annual energy production of the WPP is strongly related to Fig. 2, where the losses occurring in a WPP are shown. It becomes obvious that in order to determine the AEP of the WPP, one need to determine the energy captured by the WT blades and the losses in different stages of the system, in the path towards the offshore substation. In this paper, the HVDC transmission lines are considered to be the same regardless the technical solution adopted for the WPP (i.e. AC or DC), and are therefore assumed to have no influence on the assessment results.

With regard to Fig. 3, input to the WT blades is the site specific wind speed with certain turbulence and wind shear characteristics. The WT losses have been calculated using analytically determined loss models for each of the involved components. The same approach has been adopted for the

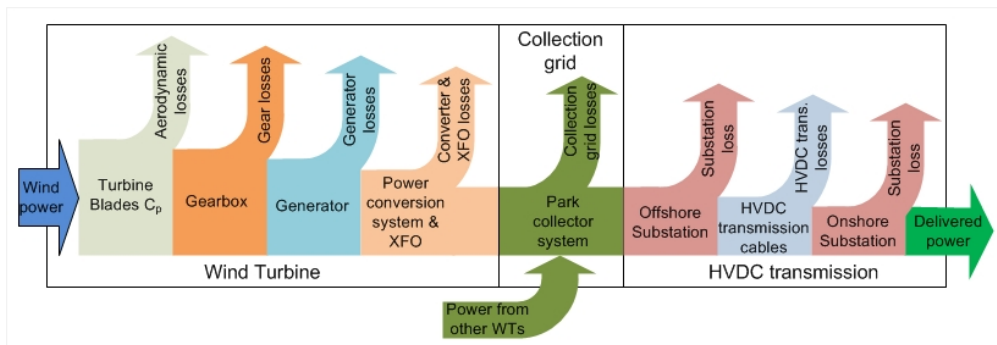


Fig. 2. Block diagram of the offshore WPP showing the losses that occur in different locations of the system.

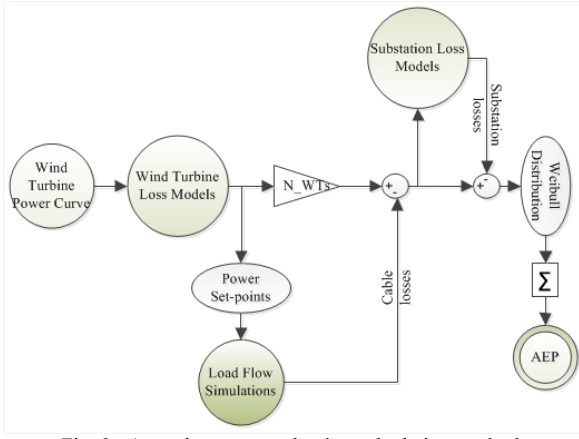


Fig. 3. Annual energy production calculation method.

substation, while for the losses in the collection grid, multiple load flow simulations have been performed at different wind speeds, reflecting different loading conditions as a result of varying wind speed. The Weibull distribution has been applied for quantifying the AEP of the WPP.

The AEP of different system configurations can be obtained similarly, by following the same approach used to calculate the aggregated cost. This involves isolating the losses of certain components in the base case system and replacing them with the calculated losses of the components in the new system configurations.

Just as for calculating the BOM cost, it is obvious that for accurate determination of losses one needs to perform detailed design work and modeling of the involved components.

### C. Need for Analytically Determined Loss Models

CoE calculation requires accurate data regarding the BOM cost and annual energy loss (AEL). Both the AEL and BOM cost involves component specific design. For exemplification purpose, this paper is focusing on the power conversion system (PCS), for which a design example is presented.

As can be seen in Fig. 4, in order to perform a design of the PCS, its loading must be determined. Based on the loading conditions, appropriate devices can be chosen and the overall losses in the converter can be determined. Design must assure that the temperature increase in the converter does not exceed the maximum specified limit.

The loading information of the PCS can be obtained in two major ways, namely by using time-step simulations with

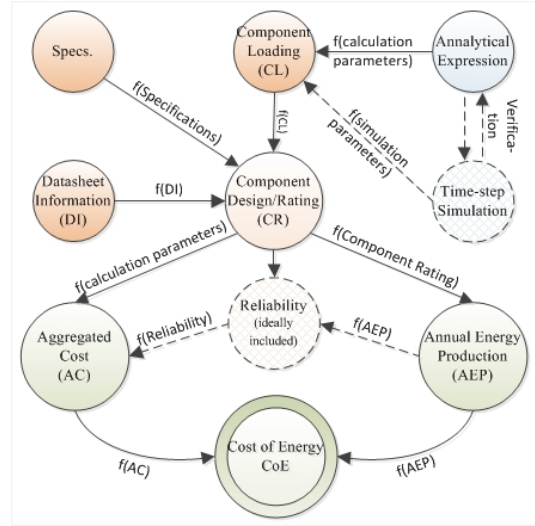


Fig. 4. Diagram of the CoE Calculation Algorithm.

specialized software or by obtaining closed form analytical equations based on converter equivalent circuit and converter switching states. Since the losses need to be determined from zero power to nominal power, it becomes obvious that the approach based on time-step simulations might be very time consuming for a large number of designs and configurations. Even for a single design, one would need to perform several simulations at different power levels (i.e. given different wind speeds). Consequently, the number of power levels at which the loading is calculated is limited by the number of simulations that one will carry out.

As opposed to time-step simulations, even though some time will be spent on developing the models, the approach based on closed form analytical equations is much more convenient when it comes to simulating different designs and configurations, because of the much lower computation time, and increased configurability and automation level. Moreover, in contrast with time-step simulations, closed form analytical loading determination allows calculation of losses from zero power to nominal power with no restrictions on the number of power steps.

Given these considerations, a contribution of this paper is that it considers the approach based on analytically determined closed form equations for the converter loading. In this context, parametric expressions have to be obtained, as follows:

$$\text{Component Rating} = f(\text{Specifications}, \text{Device Catalogue}) \quad (5)$$

$$\text{Losses} = f(\text{Component Rating}, \text{Weibull Distribution}) \quad (6)$$

$$\text{BoM} = f(\text{Component Rating}) \quad (7) \quad \text{Reliability} = f(\text{Component Rating}, \text{Losses}) \quad (8)$$

$$\text{O\&M Cost} = f(\text{Reliability}) \quad (9)$$

Ideally, one would also consider a parametric expression for reliability, since it has an influence on the O&M cost of the system.

In this paper the focus will be on losses and cost without taking into consideration reliability considerations. However,

considerable variations in the O&M cost can be associated with reliability issues. It is therefore recommended to consider reliability when calculating the CoE.

Section IV presents an example of obtaining parametric expressions as the ones presented above. For completeness of the CoE calculation algorithm a similar algebra needs to be performed with regard to reliability.

### III. CONSIDERED TECHNOLOGY OPTIONS

With regard to Fig. 5, different options can be considered for the WT structure, the substation structure and the layout of the collection grid, as explained below.

#### A. Base Case System Layout

A generic architecture of the considered system is depicted in Fig. 5 and as can be seen, it considers a WPP formed by four clusters connected to shore through HVDC transmission. The base case system considers typical 8 MW WTs with full-scale back-to-back converters, having the power curve as shown in Fig. 6. All the other WT configurations have their own power curves. A typical 33 kV AC collection grid and a typical HVDC offshore substation based on two-level voltage source converters are considered as well for the base case configuration [7].

#### B. Wind Turbine and Substation Configurations

The PCS of the WT considers three different topologies. For the AC WT, a full-scale back-to-back voltage source converter (VSC) based on three-level neutral point clamped (NPC) technology is adopted.

The AC WT can be modified by replacing the grid side VSC with a DC/DC converter, so that a DC WT is obtained. Two different topologies have been considered in this work for the DC/DC converter inside the WT, namely the Three-phase Single Active Bridge converter (SAB3) and the Three-phase Dual Active Bridge converter (DAB3) [37].

For the substation PCS two different topologies have been

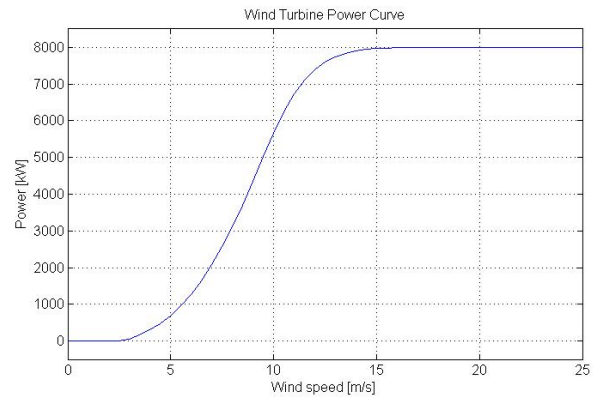


Fig. 6. Power curve of the considered base case wind turbine.

considered. In case of an AC collection grid, the substation converter is built based on the well-known two-level technology. In the case of a DC collection grid, the substation can be modified by replacing the typical AC/DC structure with a DC/DC conversion stage which, in this paper, is considered to be a three-phase Dual Active Bridge converter (DAB3). Two different options have been considered in this paper for the location of the offshore substation, namely in the center and outside center of the WPP.

#### C. Collection Grid Configurations

Two different options have been considered for the layout of the collection grid, namely the radial configuration and the star configuration, as depicted in Fig. 7. The collection grid is operated at 33 kV AC using 3-core XLPE copper cables and  $\pm 35$  kV DC using triple extruded bi-pole polymer cables.

### IV. EXAMPLE OF PARAMETRIC EXPRESSION DETERMINATION

As it was previously mentioned, this paper is focused on obtaining parametric expressions only for the losses and cost of the system. The approach used to determine such closed form expressions for the full-scale back-to-back three-level

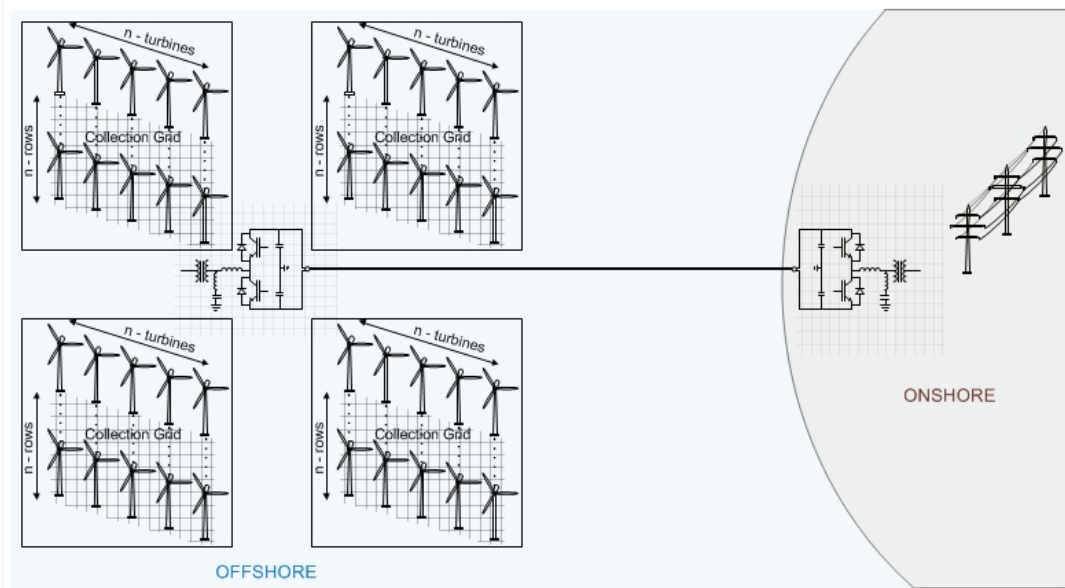


Fig. 5. Generic layout of the considered offshore wind power plant connected to onshore grid through HVDC transmission.

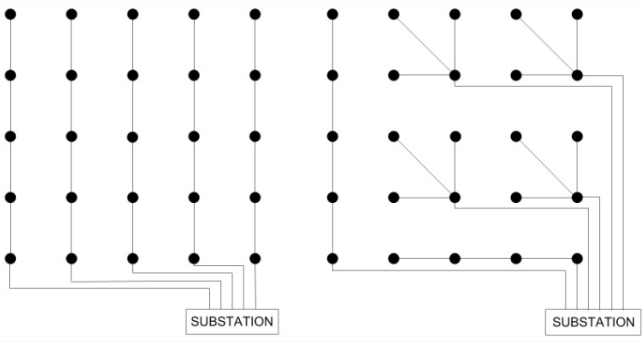


Fig. 7. Collection grid configuration for the four clusters. Radial (left) and Star (right) layouts.

NPC converter is described in detail in [36]. In the following, the closed form parametric expressions for the losses of a three-phase Dual Active Bridge DC/DC converter are derived.

A first step in determining the losses in the converter is to calculate the loading (i.e. RMS and AVERAGE values of the current) through the switching devices. Afterwards, a predesign study that takes into account thermal modeling aspects must be performed in order to choose suitable devices for which datasheet characteristics are extracted and used to calculate the losses. The power electronic switching devices are chosen so that the temperature increase for a given device type will not force the converter to operate outside the specified temperature limits. Several iteration steps might be necessary until the right switching devices are chosen.

With regard to Fig. 8, two types of power electronic devices are forming the switch in the converter, namely the IGBT and its anti-parallel Diode. Both devices will face two different types of losses, namely conduction losses and switching losses. For the Diode, the switching losses are represented by the so called reverse recovery loss. The following equations approximate the previously mentioned losses.

$$P_{cond\_IGBT} = V_{t0}(T) \cdot I_{avg\_IGBT} + R_t(T) \cdot I_{rms\_IGBT}^2 \quad (10)$$

$$P_{cond\_D} = V_{d0}(T) \cdot I_{avg\_D} + R_d(T) \cdot I_{rms\_D}^2 \quad (11)$$

$$P_{sw\_IGBT} = V_{DC} \cdot E_{sw\_IGBT} \cdot f_{sw} \cdot I_{sw\_avg\_IGBT} \quad (12)$$

$$P_{sw\_D} = V_{DC} \cdot E_{sw\_D} \cdot f_{sw} \cdot I_{sw\_avg\_D} \quad (13)$$

In the above equations the following notations have been used:

- $V_{t0}(T) / V_{d0}(T)$ : is the temperature dependent threshold voltage of the IGBT / Diode;
- $R_t(T) / R_d(T)$ : is the temperature dependent resistances of the IGBT / Diode;
- $I_{avg\_IGBT} / I_{avg\_D}$ : is the average current of the IGBT / Diode;
- $I_{rms\_IGBT} / I_{rms\_D}$ : is the RMS current of the IGBT / Diode;
- $E_{sw\_IGBT} / E_{sw\_D}$ : is the sum of the p.u. VA IGBT / Diode turn-on and turn-off switching energy;
- $I_{sw\_avg\_IGBT} / I_{sw\_avg\_D}$ : is the average switched current of the IGBT / Diode;
- $V_{DC}$ : is the DC-link voltage of the converter;
- $f_{sw}$ : is the switching frequency of the converter;

The converter will also experience losses in the medium frequency transformer, namely copper losses and core losses, as follows [38].

$$P_{cu} = 3 \sum_{h=1}^N R(f_h) \cdot I(f_h)^2 \quad (14)$$

$$P_{core} = M_{core} \cdot k_1 \cdot (\Delta B)^{\beta-\alpha} \cdot f_{sw} \cdot \sum_m \left| \frac{B_{m+1} - B_m}{t_{m+1} - t_m} \right|^\alpha \cdot (t_{m+1} - t_m) \quad (15)$$

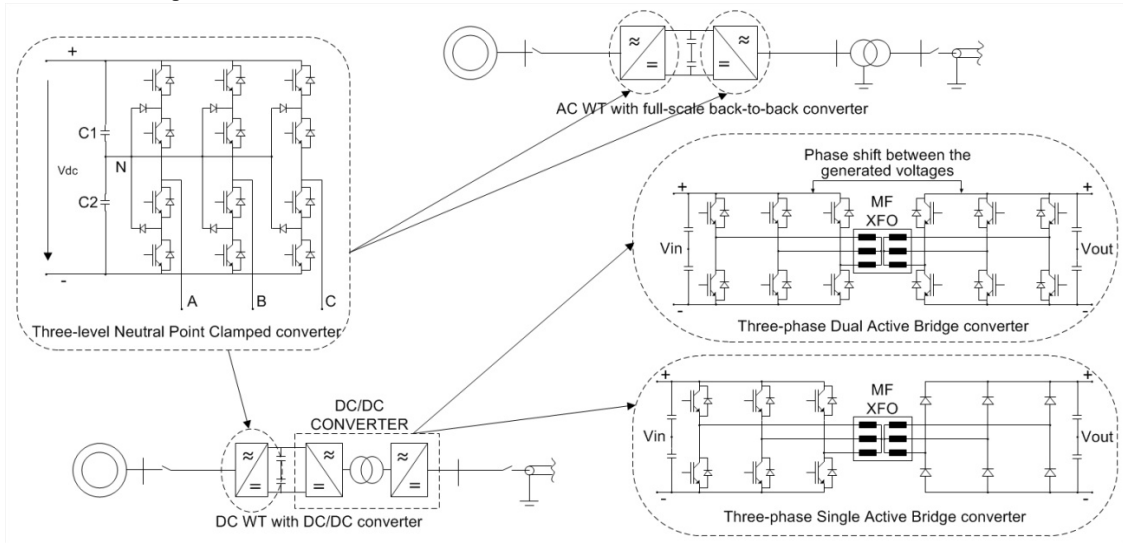


Fig. 8. Wind turbine internal structures considered in this paper.

$$k_1 = \frac{k}{2^{(\beta+1)} \cdot \pi^{(\alpha-1)} \cdot \left(0.2761 + \frac{1.7061}{\alpha+1.354}\right)} \quad (15.1)$$

In the above equations the following notations have been used:

- $R(f_h)$ : is the winding resistance at the frequency  $f_h$ ;
- $I(f_h)$ : is the RMS current component at the frequency  $f_h$ ;
- $\alpha, \beta, k$ : Steinmetz parameters, obtainable from the core material data sheets;
- $M_{core}$ : is the core weight, obtainable from the transformer design;
- $B$ : is the core flux density;
- $\Delta B$ : is the flux density variation;
- $f_{sw}$ : is the switching frequency of the converter;

It can be noticed from the above equations that for calculating the losses of the medium frequency transformer, one needs knowledge of the RMS current through the transformer at different frequency components along with the resistance for that component, the Steinmetz parameters  $\alpha, \beta$  and  $k$ , the core size  $M_{core}$  and the flux trajectory.

The RMS current through the transformer can be found from the operating principles of the converter, the Steinmetz parameters can be obtained from the core material data sheets, the core weight is obtained from the transformer design process while the flux trajectory can be obtained from the applied voltage waveforms on the transformer, corresponding to the operating principles of the converter.

The losses in the input and output capacitors are much lower than the other types of losses occurring in the converter and are therefore not considered in this analysis.

The loading through the converter's switches is determined based on the operating principles of the converter, which will determine the shape of the applied voltage across the leakage inductance of the transformer ( $L_{leak}$ ). Using the equivalent circuit of the converter and the converter switching states, six different operation modes can be distinguished in the waveforms shown in Fig. 9.

Two sets of equations can be written using the equivalent circuit and the converter waveforms [37]. One set of equations is applicable for phase shift angles (i.e. between the

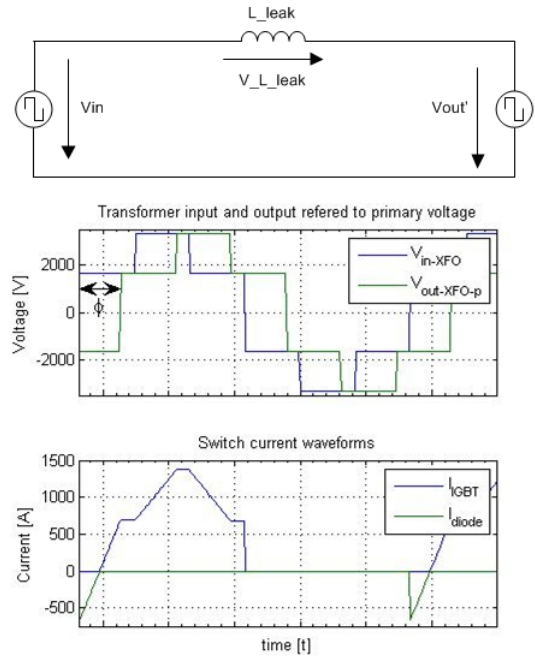


Fig. 9. Equivalent circuit and operating waveforms of DAB converter.

applied voltages on the primary side and secondary side of the medium frequency transformer)  $\varphi < \pi/3$  and the other set of equations for phase shift angles  $\varphi > \pi/3$ . Since the converter is able to operate in both buck and boost modes, independent of the transformation ratio of the medium frequency transformer, it becomes obvious that the above mentioned equations have to be written for three different DC transformation ratios (i.e.  $d=1, d<1$ , and  $d>1$ ). Depending on its DC transformation ratio, the converter can operate in the soft switching region or in the hard switching region.

Using the two aforementioned sets of equations, the relations describing the loading of the converter were derived and are presented below for the simplest case with DC transformation ratio equal to 1 and for phase shift angles smaller than  $\pi/3$ . The full set of equations for unity DC transformation ratio is presented in the APPENDIX.

$$I_{avg\_IGBT} = \frac{(4\pi^2 - 18\varphi^2 d - 9\varphi^2 d^2 - 8d\pi^2 + 4d^2\pi^2 + 12d^2\pi\varphi + 36\pi d\varphi) \cdot V_{ip}}{108 \cdot (1 + d) \cdot L_{leak} \omega \pi} \quad (16)$$

$$I_{rms\_IGBT} = \frac{\sqrt{2}}{54} \cdot \left( \left( \frac{23d^3\pi^3 - 27\varphi^3 d^3 - 36\varphi d^3\pi^2 + 54\pi d^3\varphi^2 + 108\pi d^2\varphi^2 - 39d^2\pi^3 - 81\varphi^3 d^2}{\omega^2 L_{leak}^2 \cdot (1 + d) \cdot \pi} \right) \cdot V_{ip}^2 \right. \\ \left. + \left( \frac{72\varphi d^2\pi^2 + 9d\pi^3 + 162\pi d\varphi^2 - 81\varphi^3 d - 36\varphi d\pi^2 + 7\pi^3}{\omega^2 L_{leak}^2 \cdot (1 + d) \cdot \pi} \right) \cdot V_{ip}^2 \right)^{\frac{1}{2}} \quad (17)$$

$$I_{avg\_D} = -\frac{V_{ip} \cdot (-2\pi + 2d\pi - 3d\varphi)^2}{108 \cdot (1 + d) \cdot \omega \pi L_{leak}} \quad (18)$$

$$I_{rms\_D} = \frac{\sqrt{2}}{54} \cdot \sqrt{\frac{V_{ip}^2(-2\pi + 2d\pi - 3d\varphi)^3}{\omega^2 L_{leak}^2 \cdot (1+d) \cdot \pi}} \quad (19)$$

$$I_{sw\_avg\_IGBT} = -\frac{V_{ip} \cdot (-2\pi + 2d\pi - 3d\varphi)}{9\omega L_{leak}} \quad (20)$$

$$I_{sw\_avg\_D} = -I_{sw\_avg\_IGBT} \quad (21)$$

## V. STUDY CASE

The evaluation methodology has been applied for the considered technology options presented above, but the analysis can be further extended for a more comprehensive study.

The size of the offshore WPP considered in this paper is 800 MW and consists of 100 WTs, rated 8 MW each. Two options have been considered for the PCS of the DC WT (i.e. SAB3 converter and DAB3 converter) while for the AC WT the three-level NPC converter has been considered. A DAB3 converter has been considered for the substation PCS. The DC/DC converters operate at a switching frequency of 1 kHz. For the collection grid two configurations have been considered (i.e. radial and star configuration) using 33kV AC 3-core XLPE copper cables and  $\pm 35$  kV DC triple extruded bi-pole polymer cables. The site conditions used in this study case are presented in Fig. 10.

With the evaluation methodology and the technology options presented above the assessment results are presented in Fig. 11. The following notations correspond to the configurations shown on the figure.

Configuration	Substation position	Collection grid layout	Technology
1a / 4a	Center / Outside Center	Radial	AC
1b / 4b	Center / Outside Center	Star	AC
2a / 5a	Center / Outside Center	Radial	DAB3
2b / 5b	Center / Outside Center	Star	DAB3
3a / 6a	Center / Outside Center	Radial	SAB3
3b / 6b	Center / Outside Center	Star	SAB3

It can be noticed that from a CoE point of view, the most appropriate solution seems to be configuration “6a”, which has a radial collection grid configuration, a DAB3-based substation located in the outside center of the WPP and a SAB3-based DC WT. The average CoE improvement is approximately 1.4%, but it can go as big



Fig. 10. Study case site conditions.

as 2.6% or as low as almost 0%. It is obvious that radial grid configuration is superior in terms of CoE across all the considered cases. The variations in the CoE of each configuration are the result of best and worst case scenarios for both aggregated cost and AEP of the WPP.

## VI. CONCLUSIONS

In this paper a CoE evaluation tool based on closed form equations of losses in the power conversion system of AC and DC offshore WPPs was presented. The analysis performed by the CoE tool involves the combined effect of WT aspects, collection grid aspects and substation aspects. The contribution of this paper is given by the approach used to calculate the losses in the power electronic conversion system of the WT and substation, namely by obtaining closed form expressions for systems losses. The main benefits of this approach are the increased flexibility, configurability, automation level, and computation speed of the CoE evaluation tool. This work is intended to be helpful in assessing the benefits of adopting DC technologies compared to conventional AC solutions, as proven by the results shown in Fig. 11.

The background on CoE calculation was presented in section II, where the need for accurate closed form expressions of the power electronic converters loading was emphasized and explained. After presenting the considered technology options in section III, parametric expressions

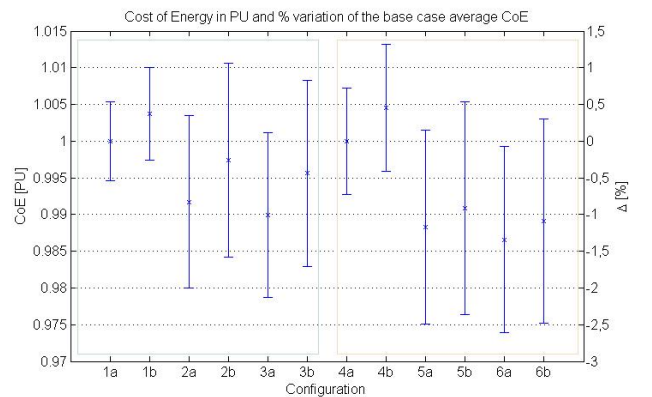


Fig. 11. CoE assessment results.

for the loading of a three-phase Dual Active Bridge converter were obtained in section IV. Section V presents a study case where the benefits of DC technologies are emphasized in terms of CoE, proving the hypothesis given in the introductory section.

Further work needs to serve a completion of the algorithm presented in this paper, by considering the influence of component reliability on the CoE results. This should be done similar to the approach taken for the loss evaluation, by means of parametric expressions. Besides assessing the most appropriate system layout, the use of this tool might also be extended to assess the system in terms of voltage levels.

#### REFERENCES

- [1] R. Gruet, "Wind energy and EU climate policy. Achieving 30% lower emissions by 2020," European Wind Energy Association (EWEA), October 2011.
- [2] Global Wind Energy Council (GWEC), "Global Wind Report - Market update 2010," Global Wind Energy Council (GWEC), 2011.
- [3] A. Arapogianni, J. Moccia, D. Williams and J. Phillips, "Wind in our Sails. The coming of Europe's offshore wind energy industry," European Wind Energy Association (EWEA), 2011.
- [4] The Crown Estate, "UK Offshore Wind Report 2011," The Crown Estate, 2011.
- [5] P. Sandeberg and L. Stenius, "Large scale Offshore Wind Power Energy evacuation by HVDC Light®," in *European Wind Energy Conference and Exhibition (EWECE)*, 2008.
- [6] N. Flourentzou, V. G. Agelidis and G. D. Demetriades, "VSC-Based HVDC Power Transmission Systems: An Overview," *IEEE TRANSACTIONS ON POWER ELECTRONICS*, vol. 24, no. 3, March 2009.
- [7] M. P. Bahrman and B. K. Johnson, "The ABCs of HVDC Transmission Technology," *IEEE power & energy magazine*, pp. 31-44, March/April 2007.
- [8] Energinet.dk, Svenska Kraftnät, and Vattenfall Europe Transmission, "An Analysis of Offshore Grid Connection at Kriegers Flak in the Baltic Sea - Joint Pre-feasibility Study," 2009.
- [9] T. Haileselassie, M. Molinas and T. Undeland, "Multi-Terminal VSC-HVDC System for Integration of Offshore Wind Farms and Green Electrification of Platforms in the North Sea," 2008. [Online]. Available: <http://www.elkraft.ntnu.no/en/Papers2008/Haileselassie-norpie08.pdf>. [Accessed January 2012].
- [10] T. Haileselassie and K. Uhlen, "Power Flow Analysis of Multi-terminal HVDC Networks," in *IEEE Trondheim PowerTech*, September 2011.
- [11] E. Veilleux and B.-T. Ooi, "Power Flow Analysis in Multi-Terminal HVDC Grid," *Power Systems Conference and Exposition*, pp. 1-7, 20-23 May 2011.
- [12] L. Xu, B. Williams and L. Yao, "Multi-Terminal DC Transmission Systems for Connecting Large Offshore Wind Farms," in *IEEE Power and Energy Society General Meeting - Conversion and Delivery of Electrical Energy in the 21st Century*, 2008.
- [13] J. Zhu and C. Booth, "Future Multi-Terminal HVDC Transmission Systems using Voltage Source Converters," in *45th International Universities Power Engineering Conference (UPEC)*, 2010.
- [14] L. Xu, L. Yao and M. Bazargan, "DC Grid Management of a Multi-Terminal HVDC Transmission System for Large Offshore Wind Farms," in *International Conference on Sustainable Power Generation and Supply (SUPERGEN)*, 2009.
- [15] L. Max and S. Lundberg, "System Efficiency of a DC/DC Converter-based Wind Farm," in *Wind Energy Journal*, 2008.
- [16] S. Lundberg, "Wind Farm Configuration and Energy Efficiency Studies - Series DC versus AC Layouts," Sweden, 2006.
- [17] O. Martander, "DC grid for wind farms," Department of Electric Power Engineering, Chalmers University of Technology, Goteborg, 2002.
- [18] S. Norrga, "An Experimental Study of a Soft-switched Isolated AC/DC Converter without Auxiliary Circuit," in *35th Annual IEEE Power Electronics Specialists Conference*, Aachen, 2004.
- [19] F. Iov, F. Blaabjerg, "Power Electronics and Control for Wind Power Systems," in *Power Electronics and Machines in Wind Applications (PEMWA)*, 2009.
- [20] C. Meyer and R. D. Doncker, "Design of a three-phase series resonant converter for offshore DC grids," in *Proc. the 42th IEEE Industry Application Society Annual Meeting (IAS)*, 2007.
- [21] R. Steigerwald, R. D. Doncker and H. Kheraluwala, "A comparison of high power DC-DC soft-switched converter topologies," *IEEE Trans. Industry Applications*, vol. 32, no. 5, p. 1139-1145, September/October 1996.
- [22] J. Jacobs, A. Averberg and R. D. Doncker, "Multi-Phase Series Resonant DC-to-DC Converters: Stationary Investigations," in *Power Electronics Specialists Conference (PESC)*, 2005.
- [23] J. Jacobs, A. Averberg, R. D. Doncker and S. Schröder, "Multi-Phase Series Resonant DC-to-DC Converters: Transient Investigations," in *Power Electronics Specialists Conference (PESC)*, 2005.
- [24] G. Demetriades, "On small-signal analysis and control of the single-and dual active bridge topologies," Department of Electrical Engineering, Royal Institute of Technology, Stockholm, 2005.
- [25] G. Ortiz, J. Biela, D. Bortis and J. Kolar, "1 Megawatt, 20 kHz, Isolated, Bidirectional 12kV to 1.2kV DC-DC Converter for Renewable Energy Applications," 2010.
- [26] C. Dick, A. König and R. D. Doncker, "Comparison of Three-Phase DC-DC Converters vs. Single-Phase DC-DC Converters," in *7th International Conference on Power Electronics and Drive Systems (PEDS)*, 2007.
- [27] A. B. Mogstad and M. Molinas, "Power collection and integration on the electric grid from offshore wind parks," in *Nordic Workshop on Power and Industrial Electronics*, 2008.
- [28] S. Lundberg, "Evaluation of wind farm layouts," in *Nordic Workshop on Power and Industrial Electronics*, 2004.
- [29] O. Carlsson and S. Lundberg, "Integration of Wind Power by DC-Power Systems," in *PowerTech Conference*, St. Petersburg, 2005.
- [30] R. M. Dermott, G. Hassan and P. Ltd., "Investigation of Use of Higher AC Voltages on Offshore Wind Farms," in *European Wind Energy Conference and Exhibition (EWECE)*, 2009.
- [31] S. Shao and V. Agelidis, "Review of DC System Technologies for Large Scale Integration of Wind Energy Systems with Electricity Grids," in *Energies*, 2010.
- [32] L. Max, "Design and Control of a DC Collection Grid for a Wind Farm," CHALMERS UNIVERSITY OF TECHNOLOGY, Goteborg, 2009.
- [33] C. Meyer, M. Höing, A. Peterson and R. D. Doncker, "Control and Design of DC Grids for Offshore Wind Farms," *Transactions on Industry Applications*, vol. 43, no. 6, November/December 2007.
- [34] L. Fingersh, M. Hand and A. Laxson, "Wind Turbine Design Cost and Scaling Model," National Renewable Energy Laboratory, 2006.
- [35] C. Meyer, "Key Components for future offshore DC grids," *Aachener Beiträge des ISEA*, 2007.
- [36] L. Helle, "Modeling and Comparison of Power Converters for Doubly Fed Induction Generators in Wind Turbines," Institut for Energiteknik, Aalborg Universitet, Aalborg, 2007.
- [37] R. W. A. A. De Doncker, D. M. Divan and M. H. Kheraluwala, "A Three-phase Soft-Switched High-Power-Density dc/dc Converter for High-Power Applications," *IEEE Transactions on Industry Applications* 27, pp. 63-73, 1991.
- [38] J. Li, T. Abdallah and C. R. Sullivan, "Improved Calculation of Core Loss With Nonsinusoidal Waveforms," in *IEEE Industry Applications Society Annual Meeting*, 2001.

APPENDIX

Two sets of equations can be written using the equivalent circuit and the converter current waveforms [37]. Each set of equations describes six operation modes for the converter. One set of equations is applicable for  $\varphi < \frac{\pi}{3}$  and another set of equations for  $\varphi > \frac{\pi}{3}$ . One equation is presented below as example, with  $i_{mod1}(\theta)$  being the converter current in the first operating mode,  $V_{ip}$  the input voltage of the converter,  $d$  the DC transformation ratio,  $\theta = \omega t$  and  $\omega = 2\pi f$ , where  $f$  is the switching frequency:

$$i_{mod1}(\theta) = \frac{V_{ip} \cdot (1 + 2d) \cdot \theta}{3 \cdot \omega \cdot L_{leak}} + i_p(0) \quad (1)$$

The value of the current at the instant 0 must be determined using the current expressions, in order to calculate the converter's average input current and power, as follows:

For  $\varphi < \frac{\pi}{3}$ :

$$i_p(0) = -\frac{V_{ip} \cdot (2\pi - 2d\pi + 3d\varphi)}{9\omega L_{leak}} \quad (2)$$

A similar expression can be obtained for  $\varphi > \frac{\pi}{3}$ .

The average input current and power for  $\varphi < \frac{\pi}{3}$  were calculated based on the two aforementioned sets of equations, as follows [37]:

$$I_{avg\_IGBT} = \frac{(4\pi^2 - 9\pi^2 d + 3\pi^2 d^2 + 18d^2 \varphi \pi + 42\pi d \varphi - 18d^2 \varphi^2 - 27d\varphi^2) \cdot V_{ip}}{108 \cdot (1 + d) \cdot L_{leak} \omega \pi} \quad (7)$$

$$I_{rms\_IGBT} = \frac{\sqrt{2}}{54} \cdot \left( \left( \frac{29d^3 \pi^3 - 108\varphi^3 d^3 + 162d^3 \pi \varphi^2 - 81d^3 \pi^2 \varphi + 216\pi d^2 \varphi^2 - 216d^2 \varphi^3 + 45d^2 \varphi \pi^2}{\omega^2 L_{leak}^2 \cdot (1 + d) \cdot \pi} \right) \cdot V_{ip}^2 + \left( \frac{-37d^2 \pi^3 - 135d\varphi^3 - 18\pi^2 d \varphi + 5\pi^3 d + 162\varphi^2 d \pi + 7\pi^3}{\omega^2 L_{leak}^2 \cdot (1 + d) \cdot \pi} \right) \cdot V_{ip}^2 \right)^{\frac{1}{2}} \quad (8)$$

$$I_{avg\_D} = -\frac{V_{ip} \cdot (4\pi^2 - 7\pi^2 d)^2 + 5\pi^2 d^2 - 18d^2 \varphi \pi + 6\pi d \varphi + 18d^2 \varphi^2 + 9d\varphi^2}{108 \cdot (1 + d) \cdot \omega \pi L_{leak}} \quad (9)$$

$$I_{rms\_D} = \frac{\sqrt{2}}{54} \cdot \left( \left( \frac{14d^3 \pi^3 - 108\varphi^3 d^3 - 81d^3 \pi^2 \varphi + 162d^3 \pi \varphi^2 - 25\pi^3 d^2 - 54d^2 \varphi^3 + 72d^2 \varphi \pi^2}{\omega^2 L_{leak}^2 \cdot (1 + d) \cdot \pi} \right) \cdot V_{ip}^2 + \left( \frac{-27\pi d^2 \varphi^2 - 81\pi d \varphi^2 + 17\pi^3 d + 9\pi^2 d \varphi + 27\varphi^3 d - 8\pi^3}{\omega^2 L_{leak}^2 \cdot (1 + d) \cdot \pi} \right) \cdot V_{ip}^2 \right)^{\frac{1}{2}} \quad (10)$$

$$I_{sw\_avg\_IGBT} = -\frac{V_{ip} \cdot (-2\pi + 3d\pi - 6d\varphi)}{9\omega L_{leak}} \quad (11)$$

$$I_{sw\_avg\_D} = \frac{V_{ip} \cdot (3\varphi - 3\pi + d\pi)}{9\omega L_{leak}} \quad (12)$$

$$I_{avg} = \frac{V_{ip} d \varphi \cdot (4\pi - 3\varphi)}{9\pi \omega L_{leak}} \quad (3)$$

$$P_{avg} = \frac{V_{ip}^2 d \varphi \cdot (4\pi - 3\varphi)}{6\pi \omega L_{leak}} \quad (4)$$

A similar set of equations can be written for  $\varphi > \frac{\pi}{3}$ .

The required phase shift angle for transferring a certain amount of power, for  $\varphi > \frac{\pi}{3}$  is calculated as follows:

$$\varphi = \frac{6d\pi V_{ip} - 2 \cdot \sqrt{7d^2 \pi^2 V_{ip}^2 - 36d P_{in} \pi \omega L_{leak}}}{12d V_{ip}} \quad (5)$$

A similar set of equations can be written for  $\varphi > \frac{\pi}{3}$ .

The current zero crossing angle for  $\varphi > \frac{\pi}{3}$  is equal to the one for  $\varphi < \frac{\pi}{3}$ , since the DC transformation ratio  $d=1$ , and is shown below.

$$\gamma = \frac{-2\pi + 2d\pi - 3d\varphi}{3 \cdot (1 + d)} \quad (6)$$

The loading through the converter for  $\varphi > \frac{\pi}{3}$  is given by the following set of equations: